Journal of Multidisciplinary Engineering Science and Technology (JMEST)
ISSN: 2458-9403
Vol. 11 Issue 3, March - 2024

Effect Of Material Selection On The Generation Of Electric Potential Of Piezoelectric Prismatic Inclusion Embedded In The Grounded & Ungrounded Plate

Mehmet SAHIN
Department of Mathematical Engineering, Yildiz Technical University, Istanbul, Turkey
e-mail: mehmet0.sahinn@gmail.com

Ulku Babuscu Yesil
Department of Mathematical Engineering, Yildiz Technical University, Istanbul, Turkey
e-mail : ubabuscu@yildiz.edu.tr

***Abstract*— In this study, the plate which contains piezoelectric prismatic inclusion under bending effect is studied. The plate is simply supported and the electric potential is non-zero (ungrounded) and zero (grounded) configurations are examined. It is aimed to investigate the effect of material selection on the electric potential production of the piezoelectric prismatic inclusion embedded in the plate for both configurations. The mathematical modeling of the problem is formulated using the piecewise-homogeneous body model within the framework of the exact 3D equations of the electro elasticity theory. It is assumed that ideal contact conditions prevail at the interface between the piezoelectric inclusion and the matrix material. The effects of various material of matrix, various material of inclusion and geometric parameters of the plate on the generation of electric potential of the embedded piezoelectric prismatic inclusion for the given boundary conditions, contact conditions and loading condition are examined and discussed for both problems.**

Keywords*— piezoelectric material; inclusion; plate; electric potential; grounded; finite element method.

I. INTRODUCTION

Parallel to technological progress in today's world, numerous devices or gadgets are being developed and introduced for social use. Especially with the increasing knowledge of technological materials and the development of new manufacturing methods, the use of these materials in technology is becoming more and more widespread. In recent years, smart materials can be cited as an example of these rapidly growing technological materials. The main feature that distinguishes these materials from conventional materials is the mutual effect of mechanical and electrical fields on the electromechanical behaviour of the material. Materials that exhibit linear properties when electrical and mechanical fields influence each other are referred to as piezoelectric materials. Piezoelectric materials also have the ability to convert mechanical movements into electrical signals or vice versa.

The use of piezoelectric components has rapidly increased in technical applications such as sensors, actuators, transducers, generators, etc. Given their widespread use, understanding the properties of these materials requires solving various problems related to structures made of piezoelectric materials [1]. Piezoelectric materials were discovered experimentally by the Curie brothers in the 1880s. The characteristic feature of these materials is the appearance of polarization (electric field) in their structure under the influence of an electric field or mechanical deformation under mechanical load [1]. In recent years, these materials are not only used as electrical harvesters, but are also increasingly used in various sensitive devices, e.g. in aerospace, automotive, mechanical and civil engineering, medical and military vehicles and equipment, etc.

Piezoelectric materials containing discontinuities in various geometric shapes have been studied by many researchers. Initially, problems with piezoelectric inclusions in different shapes for infinite medium [2-15] or 2D problems [16-20] have been addressed and studied. However, it is essential to tackle the problems in three dimensions and solve them with more accurate theories both theoretically and practically.

3D design and numerical analysis of a novel multi-degree of freedom micropositioner driven by piezoelectric stacks actuator was studied in [21]. A novel rhombic piezoelectric actuator was developed to solve the contradiction between high precision and large working stroke in the traditional parallel stage in [22]. A parametric analysis of the effective material properties of a piezoelectric macrofiber composite with a thickness of d15 and a shear of seven layers was investigated in [23]. In [24], the effective properties of a unidirectional periodic piezoelectric fiber composite were analyzed using FEM for different

loads with different boundary conditions. In [25], the electrostatic analysis of a plate with piezoelectric inclusions under the action of an axial tensile force was studied. In [26], an FE model was developed to determine the stress concentration around an elliptical hole in 3D magneto- electroelastic plates. In [27], an analysis of a piezoelectric-based composite structure was performed using FEM with a thermal analogy approach. The effect of the piezoelectric inclusions embedded in the plate under bending force using exact 3D equations of elasto- and piezo-elastostatic theories was investigated in [28].

The present study extends the study [28] by investigating both grounded and ungrounded plates for different material parameters. A 3D FEM analysis is investigated in this study for both grounded and ungrounded plates including inclusion made by piezoelectric material. The problem is modeled using the 3D exact equations of electroelasticity theory by the three-dimensional finite element method. Effect of grounding and material selection of matrix and inclusion and some geometric parameters of plate/inclusion on electrostatic analysis is studied.

II. METHOD

Consider a piezoelectric (PZT) inclusion embedded in the grounded (Problem 1) & ungrounded (Problem 2) plate. For the grounded case electric potential is taken zero and for the ungrounded case it differs from zero from all the lateral surfaces. According to the scheme in Figure 1, length, height and thickness of the inclusion are $2\ell_D, h_O$ and ℓ_3 and the total length, height and thickness of the plate to ℓ_1, h and ℓ_3, respectively.

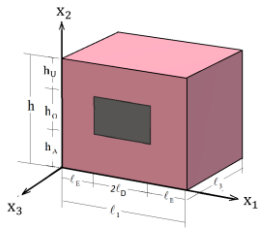

Fig. 1. The geometry of the problem

The plate is simply supported and only an uniformly distributed pressure force is acted from upper surface of the plate. The superscripts (1) and (2) represent the properties of matrix material and inclusion material, respectively. Third- and fourth-order tensors can be used for the electro-mechanical relations. However, we can utilize compact matrix notation to reduce the representations to second-order tensors, namely, indices ij or kl to a unique index as p or q, where p, q=1,2. In this case, the second-order geometrical relations can be given, as follows:

$$\sigma_p^{(m)} = c_{pq}^{(m)} s_q^{(m)} - e_{kp}^{(m)} E_k^{(m)},$$

$$D_i^{(m)} = e_{iq}^{(m)} s_q^{(m)} + \varepsilon_{ik}^{(m)} E_k^{(m)} \quad (1)$$

and in matrix form, as follows;

$$\begin{Bmatrix} \sigma_1^{(m)} \\ \sigma_2^{(m)} \\ \sigma_3^{(m)} \\ \sigma_4^{(m)} \\ \sigma_5^{(m)} \\ \sigma_6^{(m)} \\ D_1^{(m)} \\ D_2^{(m)} \\ D_3^{(m)} \end{Bmatrix} = \begin{Bmatrix} c_{11}^{(m)} & c_{12}^{(m)} & c_{13}^{(m)} & c_{14}^{(m)} & c_{15}^{(m)} & c_{16}^{(m)} \\ c_{21}^{(m)} & c_{22}^{(m)} & c_{23}^{(m)} & c_{24}^{(m)} & c_{25}^{(m)} & c_{26}^{(m)} \\ c_{31}^{(m)} & c_{32}^{(m)} & c_{33}^{(m)} & c_{34}^{(m)} & c_{35}^{(m)} & c_{36}^{(m)} \\ c_{41}^{(m)} & c_{42}^{(m)} & c_{43}^{(m)} & c_{44}^{(m)} & c_{45}^{(m)} & c_{46}^{(m)} \\ c_{51}^{(m)} & c_{52}^{(m)} & c_{53}^{(m)} & c_{54}^{(m)} & c_{55}^{(m)} & c_{56}^{(m)} \\ c_{61}^{(m)} & c_{62}^{(m)} & c_{63}^{(m)} & c_{64}^{(m)} & c_{65}^{(m)} & c_{66}^{(m)} \\ e_{11}^{(m)} & e_{12}^{(m)} & e_{13}^{(m)} & e_{14}^{(m)} & e_{15}^{(m)} & e_{16}^{(m)} \\ e_{21}^{(m)} & e_{22}^{(m)} & e_{23}^{(m)} & e_{24}^{(m)} & e_{25}^{(m)} & e_{26}^{(m)} \\ e_{31}^{(m)} & e_{32}^{(m)} & e_{33}^{(m)} & e_{34}^{(m)} & e_{35}^{(m)} & e_{36}^{(m)} \end{Bmatrix} \begin{Bmatrix} s_1^{(m)} \\ s_2^{(m)} \\ s_3^{(m)} \\ s_4^{(m)} \\ s_5^{(m)} \\ s_6^{(m)} \end{Bmatrix}$$

$$- \begin{Bmatrix} e_{11}^{(m)} & e_{21}^{(m)} & e_{31}^{(m)} \\ e_{12}^{(m)} & e_{22}^{(m)} & e_{32}^{(m)} \\ e_{13}^{(m)} & e_{23}^{(m)} & e_{33}^{(m)} \\ e_{14}^{(m)} & e_{24}^{(m)} & e_{34}^{(m)} \\ e_{15}^{(m)} & e_{25}^{(m)} & e_{35}^{(m)} \\ e_{16}^{(m)} & e_{26}^{(m)} & e_{36}^{(m)} \\ -\varepsilon_{11}^{(m)} & -\varepsilon_{12}^{(m)} & -\varepsilon_{13}^{(m)} \\ -\varepsilon_{21}^{(m)} & -\varepsilon_{22}^{(m)} & -\varepsilon_{23}^{(m)} \\ -\varepsilon_{31}^{(m)} & -\varepsilon_{32}^{(m)} & -\varepsilon_{33}^{(m)} \end{Bmatrix} \begin{Bmatrix} E_1^{(m)} \\ E_2^{(m)} \\ E_3^{(m)} \end{Bmatrix}$$

(2)

where $\sigma_p^{(m)}$, $D_i^{(m)}$, $s_q^{(m)}$ and $E_k^{(m)}$ are the corresponding components of the stress, electrical displacement, strain, and electric field vectors, respectively. Morever, $c_{pq}^{(m)}, e_{kp}^{(m)}$ and $\varepsilon_{ik}^{(m)}$ in the coefficient matrix are the mechanical, the pieozoelectric and the dielectric material parameters.

In the piezoelectric materials $E_k^{(m)}$ determined by the potential as given in Eq.3.

$$E_k^{(m)} = -\frac{\partial \Phi^{(m)}}{\partial x_k} \quad (3)$$

The electrostatic equilibrium condition can be expressed as given in Eq. (4).

$$\frac{\partial D_i^{(m)}}{\partial x_i} = 0 \quad (4)$$

The following boundary conditions

On displacement;

$$u_2^{(m)}\big|_{x_1=0;\ell_1} = u_2^{(m)}\big|_{x_3=0;\ell_3} = 0 \quad (5)$$

On stresses;

$$\sigma_1^{(m)}\big|_{x_1=0;\ell_1} = \sigma_5^{(m)}\big|_{x_1=0;\ell_1} = 0$$

$$\sigma_5^{(m)}\big|_{x_3=0;\ell_3} = \sigma_3^{(m)}\big|_{x_3=0;\ell_3} = 0$$

$$\sigma_2^{(m)}\big|_{x_2=h} = p, \sigma_6^{(m)}\big|_{x_2=h} = \sigma_4^{(m)}\big|_{x_2=h} = 0$$

$$\sigma_2^{(m)}\big|_{x_2=0} = \sigma_4^{(m)}\big|_{x_2=0} = \sigma_6^{(m)}\big|_{x_2=0} = 0 \qquad (6)$$

where $(\sigma_1 = \sigma_{11}, \sigma_2 = \sigma_{22}\ ,\ \sigma_3 = \sigma_{33}, \sigma_4 = \sigma_{23} = \sigma_{32}, \sigma_5 = \sigma_{31} = \sigma_{13}, \sigma_6 = \sigma_{12} = \sigma_{21})$

On electric potential;

For grounded plate (Problem 1)

$$\Phi^{(m)}\big|_{x_1=0;\ell_1} = \Phi^{(m)}\big|_{x_3=0;\ell_3} = 0 \qquad (7)$$

For ungrounded plate (Problem 2)

$$\Phi^{(m)}\big|_{x_1=0;\ell_1} \neq 0,\ \ \Phi^{(m)}\big|_{x_3=0;\ell_3} \neq 0 \qquad (8)$$

are satisfied. And interfaces' contact conditions are given as below:

$$u_i^{(1)} n_i^{(1)}\big|_S = u_i^{(2)} n_i^{(2)}\big|_S$$
$$\sigma_p^{(1)} n_j^{(1)}\big|_S = \sigma_p^{(2)} n_j^{(2)}\big|_S$$
$$\Phi^{(1)} \mathrm{n}^{(1)}\big|_S = \Phi^{(2)} \mathrm{n}^{(2)}\big|_S$$
$$D_i^{(1)} n_i^{(1)}\big|_S = D_i^{(2)} n_i^{(2)}\big|_S \qquad (9)$$

In Eq. (9), $n_i^{(k)}$ (k=1,2) are normal vector of surface S of the k component, and S symbolizes the surface of the inclusion.

The solution of boundary value problems, for which mathematical models are given, will be done with the 3D FE modelling. According to the method, rectangular prismatic shaped finite elements are used for both material. There are four unknowns at the nodes, three of them are displacements $u_i, (\ i = 1,2,3)$ along the three axes and one of them is electric potential Φ. The interpolation of Lagrange polynomial are used for shape functions [29]. For finite element modeling, the total electro-mechanical energy functional π is used [30, 31]:

$$\pi = \sum_{m=1}^{2} \iiint_{\Omega} \left(\frac{1}{2} G_{ijkl}^{(m)} \frac{\partial u_i^{(m)}}{\partial x_j} \frac{\partial u_k^{(m)}}{\partial x_l} + R_{ijk}^{(m)} \frac{\partial \Phi^{(m)}}{\partial x_i} \frac{\partial u_j^{(m)}}{\partial x_k} - \frac{1}{2} \varepsilon_{ij}^{(m)} \frac{\partial \Phi^{(m)}}{\partial x_k} \frac{\partial \Phi^{(m)}}{\partial x_l} \right) d\Omega_m \qquad (10)$$

A set of algebraic equations are obtained for the solution of the problems with this π functional and the Ritz technique. Since the first variation of the functional (10) is equal to zero, that is,

$$\delta\pi = \frac{\partial \pi}{\partial u_1^{(m)}} \delta u_1^{(m)} + \frac{\partial \pi}{\partial u_2^{(m)}} \delta u_2^{(m)} + \frac{\partial \pi}{\partial u_3^{(m)}} \delta u_3^{(m)} + \frac{\partial \pi}{\partial \Phi^{(m)}} \delta \Phi^{(m)} \qquad (11)$$

Within the procedures known by the Ritz method, from equation (11), a set of linear algebraic equations is obtained as given in Eq. (12).

$$\boldsymbol{K a = F} \qquad (12)$$

In (12), **K** is the coefficients (Stifness) matrix, **a** is the unknown vector and **F** is the force vector.

$$\boldsymbol{K} = \begin{bmatrix} \boldsymbol{K_{UU}} & \boldsymbol{K_{UE}^T} \\ \boldsymbol{K_{UE}} & \boldsymbol{K_{EE}} \end{bmatrix} \quad , \quad \boldsymbol{a} = \begin{bmatrix} \boldsymbol{u} \\ \mathbf{E} \end{bmatrix} \qquad (13)$$

Here, $\boldsymbol{K_{UE}}$ is the electro-elastic, $\boldsymbol{K_{UU}}$ is the mechanical and $\boldsymbol{K_{EE}}$ is the electrical global stiffness matrices, respectively, $\boldsymbol{E}$ and $\boldsymbol{u}$ are the global vectors related to the nodal electric potential and the nodal displacements. Explicit expressions of stiffness matrices are as follows:

$$\begin{Bmatrix} \boldsymbol{K_{UU}} \\ \boldsymbol{K_{UE}} \\ \boldsymbol{K_{EE}} \end{Bmatrix} = \bigcup_{e=1}^{n} \begin{Bmatrix} (\boldsymbol{K_{UU}})^{(e)} \\ (\boldsymbol{K_{UE}})^{(e)} \\ (\boldsymbol{K_{EE}})^{(e)} \end{Bmatrix},$$

$$\begin{Bmatrix} (\boldsymbol{K_{UU}})^{(e)} \\ (\boldsymbol{K_{UE}})^{(e)} \\ (\boldsymbol{K_{EE}})^{(e)} \end{Bmatrix} = \cup_{i,j=1}^{8} \begin{Bmatrix} (\boldsymbol{K_{UU}})_{ij}^{(e)} \\ (\boldsymbol{K_{UE}})_{ij}^{(e)} \\ (\boldsymbol{K_{EE}})_{ij}^{(e)} \end{Bmatrix} \qquad (14)$$

and

$$(\boldsymbol{K_{UU}})_{ij}^{(e)} = \iiint_{\Omega_e} \left(\boldsymbol{B_j^{(e)}}\right)^T \boldsymbol{D^{(e)}} \boldsymbol{B_i^{(e)}} \boldsymbol{d\Omega_e},$$

$$(\boldsymbol{K_{UE}})_{ij}^{(e)} = \iiint_{\Omega_e} \tilde{\boldsymbol{e}}^{(e)} \boldsymbol{B_i^{(e)}} \boldsymbol{C_j^{(e)}} \boldsymbol{d\Omega_e}$$

$$(\boldsymbol{K_{EE}})_{ij}^{(e)} = \iiint_{\Omega_e} \tilde{\boldsymbol{\varepsilon}}^{(e)} \boldsymbol{C_i^{(e)}} \boldsymbol{C_j^{(e)T}} \boldsymbol{d\Omega_e}$$

$$\boldsymbol{B_j^{(e)}} = \begin{pmatrix} \frac{\partial N_j^{(e)}}{\partial x_1} & 0 & 0 \\ 0 & \frac{\partial N_j^{(e)}}{\partial x_2} & 0 \\ 0 & 0 & \frac{\partial N_j^{(e)}}{\partial x_3} \\ \frac{\partial N_j^{(e)}}{\partial x_3} & 0 & \frac{\partial N_j^{(e)}}{\partial x_1} \\ 0 & \frac{\partial N_j^{(e)}}{\partial x_3} & \frac{\partial N_j^{(e)}}{\partial x_2} \\ \frac{\partial N_j^{(e)}}{\partial x_2} & \frac{\partial N_j^{(e)}}{\partial x_1} & 0 \end{pmatrix}, \quad \boldsymbol{C_j^{(e)}} = \begin{pmatrix} \frac{\partial N_j^{(e)}}{\partial x_1} \\ \frac{\partial N_j^{(e)}}{\partial x_2} \\ \frac{\partial N_j^{(e)}}{\partial x_3} \end{pmatrix} \qquad (15)$$

The elements of the matrices $\boldsymbol{D^{(e)}}$, $\tilde{\boldsymbol{e}}^{(e)}$ and $\tilde{\boldsymbol{\varepsilon}}^{(e)}$ show the elastic, piezoelectric and dielectric material constants, respectively. The values of these material matrices differ according to their polarization directions. For instance, if the polarization direction is Ox_2 the elements of matrices are given in (16) [30].

$$\boldsymbol{D^{(e)}} = \begin{pmatrix} \boldsymbol{c_{11}^{(e)}} & \boldsymbol{c_{13}^{(e)}} & \boldsymbol{c_{12}^{(e)}} & 0 & 0 & 0 \\ \boldsymbol{c_{13}^{(e)}} & \boldsymbol{c_{33}^{(e)}} & \boldsymbol{c_{13}^{(e)}} & 0 & 0 & 0 \\ \boldsymbol{c_{12}^{(e)}} & \boldsymbol{c_{13}^{(e)}} & \boldsymbol{c_{11}^{(e)}} & 0 & 0 & 0 \\ 0 & 0 & 0 & \boldsymbol{c_{44}^{(e)}} & 0 & 0 \\ 0 & 0 & 0 & 0 & \boldsymbol{c_{66}^{(e)}} & 0 \\ 0 & 0 & 0 & 0 & 0 & \boldsymbol{c_{44}^{(e)}} \end{pmatrix}$$

$$\tilde{\boldsymbol{e}}^{(e)} = \begin{pmatrix} \mathbf{0} & \mathbf{0} & \mathbf{0} & \mathbf{0} & \mathbf{0} & \boldsymbol{e}_{15}^{(e)} \\ \boldsymbol{e}_{31}^{(e)} & \boldsymbol{e}_{33}^{(e)} & \boldsymbol{e}_{31}^{(e)} & \mathbf{0} & \mathbf{0} & \mathbf{0} \\ \mathbf{0} & \mathbf{0} & \mathbf{0} & \boldsymbol{e}_{15}^{(e)} & \mathbf{0} & \mathbf{0} \end{pmatrix}$$

$$\tilde{\boldsymbol{\varepsilon}}^{(e)} = \begin{pmatrix} \boldsymbol{\varepsilon}_{11}^{(e)} & \mathbf{0} & \mathbf{0} \\ \mathbf{0} & \boldsymbol{\varepsilon}_{33}^{(e)} & \mathbf{0} \\ \mathbf{0} & \mathbf{0} & \boldsymbol{\varepsilon}_{11}^{(e)} \end{pmatrix} \quad (16)$$

The global matrix **K** are symmetric, positive definite and real, so the system given in (12) is solvable and has a unique solution. Thus, the quantities sought at the nodes are determined from the solution of this algebraic equation system.

III. NUMERICAL RESULTS

In this section, numerical results are presented to show the influence of constituent materials (inclusion and matrix) for both problems. The inclusion's material is piezoelectric material while the matrix material is metal material.

The electro-mechanical constants of some piezoelectric materials and mechanical constants of some of the metal materials employed in the calculation are given in Table 1 and Table 2, respectively.

TABLE 1. Electro-mechanical constants of some piezoelectric materials [30].
$c(10^{10}\ N/m^2), e\ (C/m^2), \varepsilon\ (10^{-8}\ C/Vm), \rho\ (Kg/m^2)$

	PZT-4	PZT-5H	$BaTiO_3$	PZT-5A	PZT-6B	PZT-8	PMN-PT
c_{11}	13.9	12.6	15.0	12.1	16.8	13.7	19.96
c_{12}	7.78	7.91	6.53	7.59	8.47	6.99	12.51
c_{13}	7.40	8.39	6.62	7.54	8.42	7.11	7.19
c_{33}	11.5	11.7	14.6	11.1	16.3	12.3	15.36
c_{44}	2.56	2.30	4.39	2.11	3.55	3.13	6.49
c_{66}	3.06	2.35	4.24	2.26	4.17	3.36	4.24
e_{31}	-5.2	-6.5	-4.3	-5.4	-0.9	-4.0	-4.3
e_{33}	15.1	23.3	17.5	15.8	7.1	13.2	17.5
e_{15}	12.7	17.0	11.4	12.3	4.6	10.4	11.4
ε_{11}	0.646	1.505	0.987	0.811	0.360	0.797	0.987
ε_{33}	0.562	1.302	1.116	0.735	0.342	0.514	1.116
ρ	7500	7500	5700	7750	7550	7600	8100

TABLE 2. Mechanical constants of some selected metals.

Metal	Al	St	Mg	Ti	W
$E\ (GPa)$	70	207	45	107	407
$\rho\ (Kg/m^2)$	2707	7850	1740	4540	19300
υ	0.33	0.3	0.29	0.34	0.28

Dimensionless values are specified for numerical calculations. The expressions for the dimensionless displacements u_1, u_2 and u_3 in the directions Ox_1, Ox_2 and Ox_3 as well as the dimensionless electric potential ϕ are given in Eq. (17).

$$\tilde{u}_1 = \frac{c_{44}^{PZT} u_1}{p\ell_1},\quad \tilde{u}_2 = \frac{c_{44}^{PZT} u_2}{p\ell_1},$$

$$\tilde{u}_3 = \frac{c_{44}^{PZT} u_3}{p\gamma_{31}\ell_1}, \tilde{\phi} = \frac{\phi e_{15}}{c_{44}^{PZT}\ell_1} \quad (17)$$

In (17), c_{44}^{PZT} is the material constant for piezoelectric inclusion, p is the intensity of the compressive force acting on the top surface of the thick plate, ℓ_1 (ℓ_3) is the length of the thick plate in the Ox_1 (Ox_3) direction and $\gamma_{31} = \ell_3/\ell_1$.

To test the mesh sensitivity of the solution domain, finite elements' number is changed along the three axes. The parameters N_1, N_2 and N_3 specify the number of rectangular prismatic finite elements along the axes Ox_1, Ox_2 and Ox_3, respectively. For the mesh sensitivity, PZT-5H material is used for the piezoelectric inclusion and AL material is used for the metal matrix. The volume of inclusion in the plate (V_d/V) is assumed to be constant. The parameters for the calculations are $h/\ell_1 = 0.1$, $V_d/V = 0.1875$. Figure 2 (a-c) shows the influence of N_1 on a) u_2 b) ϕ and c) σ_{11} for Problem 1. Figure 3 (a-c) shows the influence of N_2 on a) u_2 b) ϕ and c) σ_{11} for Problem 1. And Figure 4 (a-c) shows the influence of N_3 on a) u_2 b) ϕ and c) σ_{11} for Problem 1. Note that all the results obtained for Ox_2 polled axis in Figure 2-4.

Accordings to the graphs given in Figure 2-4, a limit value is obtained as the parameters increased. Approaching these limit values ensure the confidence of the mesh sensitivity in the results of the algorithms and programs we have created.

So, for the numerical results, a total of 6400 rectangular FEs are used, where the parameters are taken $N_1 = 20$, $N_2 = 16$ and $N_3 = 20$.

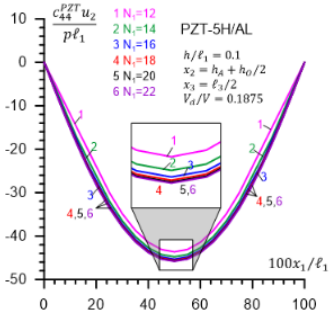

(a)

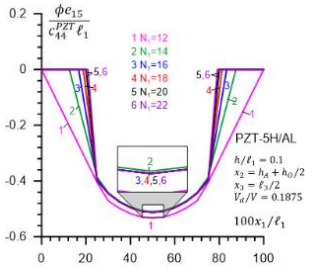

(b)

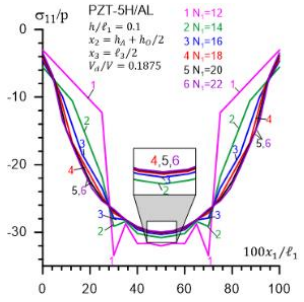

(c)

Fig. 2. Number of rectangular prismatic FEs along the $0x_1$ axis, i.e., N_1 on the values of a) u_2 b) ϕ and c) σ_{11}.

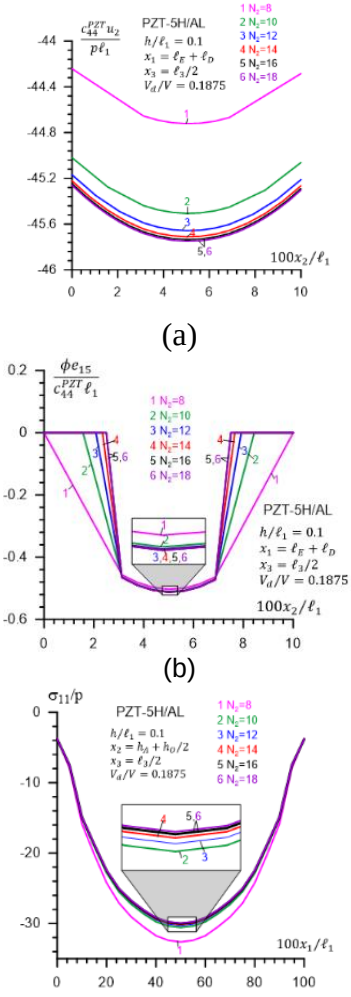

(a)

(b)

(c)

Fig. 3. Number of rectangular prismatic FEs along the $0x_2$ axis, i.e., N_2 on the values of a) u_2 b) ϕ and c) σ_{11}.

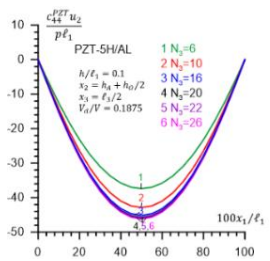

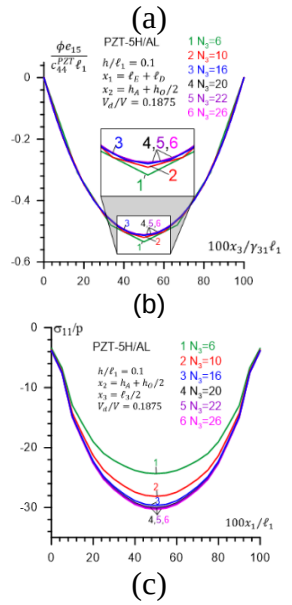

(a)

(b)

(c)

Fig. 4. Number of rectangular prismatic FEs along the $0x_3$ axis, i.e., N_3 on the values of a) u_2 b) ϕ and c) σ_{11}.

To verify our results, concentration of stresses $\boldsymbol{\sigma_{11}}$ along the axis $\mathbf{0x_1}$ in the homogeneous isotropic plate are compared with the case of the plane strain state determined by Yahnioglu [32]. We would like to point out that as the parameter $\boldsymbol{\gamma_{31}}$ increases, the plane strain state case is reached. Figure 5 shows that the values of the stress concentration at $\boldsymbol{x_3 = \ell_3/2}$ and $\boldsymbol{x_2 = 0}$ for some values of the parameter $\boldsymbol{\gamma_{31}}$. According to Figure 5, $\boldsymbol{\sigma_{11}}$ increases with increasing parameter $\boldsymbol{\gamma_{31}}$ and converges towards the relevant value for the plane strain state obtained in [32]. Thus, the accuracy of the programs and algorithms we have developed is proven again.

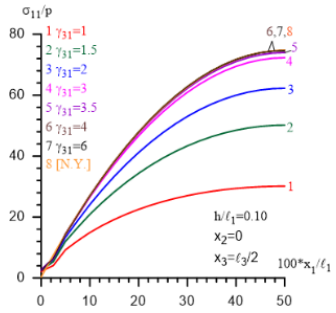

Fig. 5. Stress concentration of σ_{11} for different values of parameter γ_{31}.

We should point out that in all subsequent graphs, calculations have been made for both problems (for grounded (Problem 1) and ungrounded plate (Problem 2)). The dashed (straight) lines represent the Problem 2 (Problem 1). All the graphs are drawn in the cross-section in which the investigated effect is greatest. First, the influence of the material selection of the piezoelectric inclusion on the electric potential is examined for $\mathbf{0x_2}$ polled axis along the a) axis $\mathbf{0x_1}$ at the cross section $\mathbf{x_2 = h_A + h_0/2}$, $\mathbf{x_3 = \ell_3/2}$, b) axis $\mathbf{0x_2}$ at the cross section $\mathbf{x_1 = \ell_E + \ell_D}$, $\mathbf{x_3 = \ell_3/2}$

c) axis $\mathbf{Ox_3}$ at the cross section $\mathbf{x_1 = \ell_E + \ell_D}$, $\mathbf{x_2 = h_A + h_O/2}$ for Al matrix material for both problems in Figure 6. We should point out that the piezoelectric materials selected here are among the most commonly used materials. The maximum electric potential is reached for the material PZT-5A (PZT-4) in Problem 2 (Problem 1) and the material selection influences the values of electric potential in Problem 2 more than in Problem 1. A minimum electric potential is reached for the material PMN-PT for both problems. In Problem 1 only a negative electric potential is achived while in Problem 2 both a negative and a positive electric potential are achived.

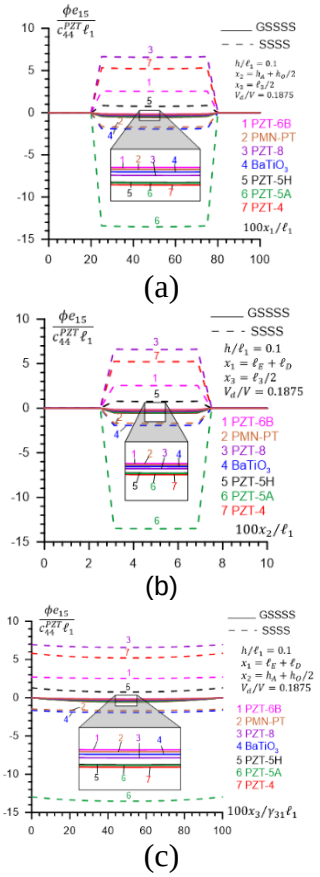

Fig. 6. Influence of different inclusion materials on the electric potential ϕ for Al matrix material for both problems along the a) $0x_1$ axis b) $0x_2$ axis c) $0x_3$ axis.

The influence of the material selection of the piezoelectric inclusion on a) the stress concentration of $\boldsymbol{\sigma_{11}}$ along the $\mathbf{Ox_1}$ axis in the cross section of $\mathbf{x_2 = h_A + h_O/2}$, $\mathbf{x_3 = \ell_3/2}$ and on b) the displacement $\mathbf{u_2}$ along $\mathbf{Ox_2}$ axis in the cross section of $\mathbf{x_1 = \ell_E + \ell_D}$, $\mathbf{x_3 = \ell_3/2}$, for Al matrix material for both problems are investigated in Figure 7. Both the stress and displacement concentrations take their absolute maximum values for the material PZT-5A and the absolute minimum values for the material PMN-PT. The stress concentration do not differ in both cases and the absolute values of the displacements are slightly larger in Problem 1 than Problem 2.

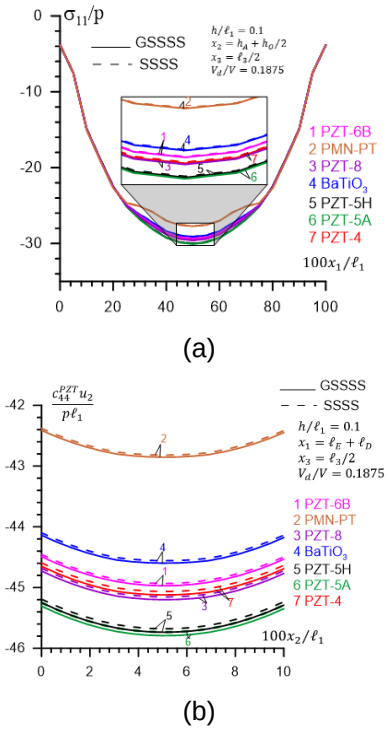

Fig. 7. Influence of various inclusion materials on the a) Stress concentration of σ_{11} along $0x_1$ axis b) Displacement of u_2 along $0x_2$ axis for Al matrix material for both problems.

In Figure 8 and 9, PZT-5H material is selected as the inclusion material, and the effects of changing the matrix material on the electric potential, stress and displacement are investigated, respectively. The influence of the matrix material selection on the electric potential is examined for $\mathbf{Ox_2}$ polled axis along the a) axis $\mathbf{Ox_1}$ at the cross section $\mathbf{x_2 = h_A + h_O/2}$, $\mathbf{x_3 = \ell_3/2}$, b) axis $\mathbf{Ox_2}$ at the cross section $\mathbf{x_1 = \ell_E + \ell_D}$, $\mathbf{x_3 = \ell_3/2}$ c) axis $\mathbf{Ox_3}$ at the cross section $\mathbf{x_1 = \ell_E + \ell_D}$, $\mathbf{x_2 = h_A + h_O/2}$ in Figure 8.

The largest absolute value of the electric potential is obtained in Problem 2 for St material, in Problem 1 for Mg material and the matrix material selection influences the values of electric potential in Problem 2 more than in Problem 1. In Problem 2 only a negative electric potential is achived while in Problem 1 both a negative and a positive electric potential are achived according to selection of matrix material.

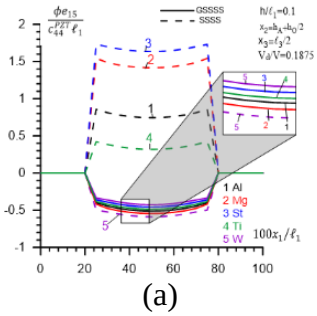

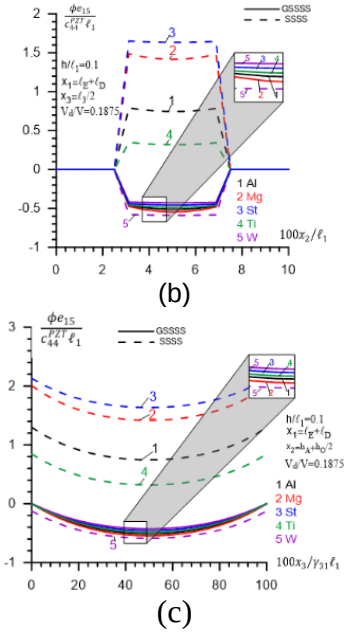

(b)

(c)

Fig. 8. Influence of matrix materials on the electric potential ϕ for both problems along the a) $0x_1$ axis b) $0x_2$ axis c) $0x_3$axis.

The influence of the matrix material selection of the plate on a) the stress concentration of $\boldsymbol{\sigma_{11}}$ along the $\mathbf{Ox_1}$ axis in the cross section of $\mathbf{x_2 = h_A + h_O/2}$, $\mathbf{x_3 = \ell_3/2}$ and on b) the displacement of $\mathbf{u_2}$ along $\mathbf{Ox_2}$ axis in the cross section of $\mathbf{x_1 = \ell_E + \ell_D}$, $\mathbf{x_3 = \ell_3/2}$, for PZT-5H inclusion/Al matrix material for both problems are investigated in Figure 9. Both the stress and displacement concentrations take their absolute maximum values for the material Tungsten (W) and their absolute minimum for the material Aluminum (Al). The stress concentrations do not differ in both cases and the absolute values of the displacements are slightly larger in Problem 1 than for Problem 2.

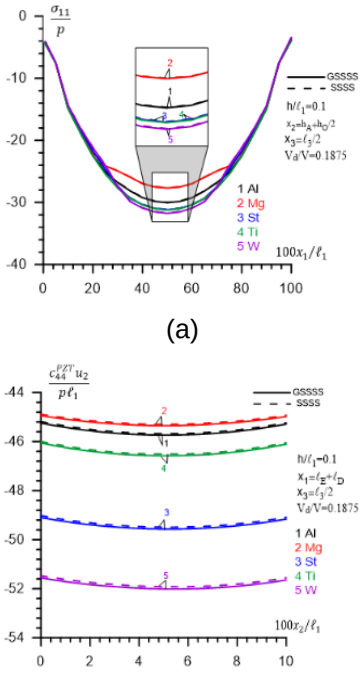

(a)

(b)

Fig. 9. Influence of various matrix materials for PZT-5H inclusion material on the a) Stress concentration of σ_{11} along Ox_1 axis b) Displacement of u_2 along Ox_2 axis for both problems.

In Figure 10, the effect of the parameter $\boldsymbol{V_D/V}$ (volume fraction of the piezoelectric inclusion in the plate) on electric potential along the axis a) $\mathbf{Ox_1}$ in the cross section of $\mathbf{x_2 = h_A + h_O/2}$, $\mathbf{x_3 = \ell_3/2}$, b) $\mathbf{Ox_2}$ in the cross section of $\mathbf{x_1 = \ell_E + \ell_D}$, $\mathbf{x_3 = \ell_3/2}$ c) $\mathbf{Ox_3}$ in the cross section of $\mathbf{x_1 = \ell_E + \ell_D}$, $\mathbf{x_2 = h_A + h_O/2}$, for PZT-5H inclusion/Al matrix material for both problems are investigated. Note that $\boldsymbol{V_D}$ indicates the volume of the piezoelectric inclusion and $\mathbf{V}$ indicates the total volume of the plate. The absolute values of the electric potential in the cross-section under consideration increase when the parameter $\boldsymbol{V_D/V}$ decreases.

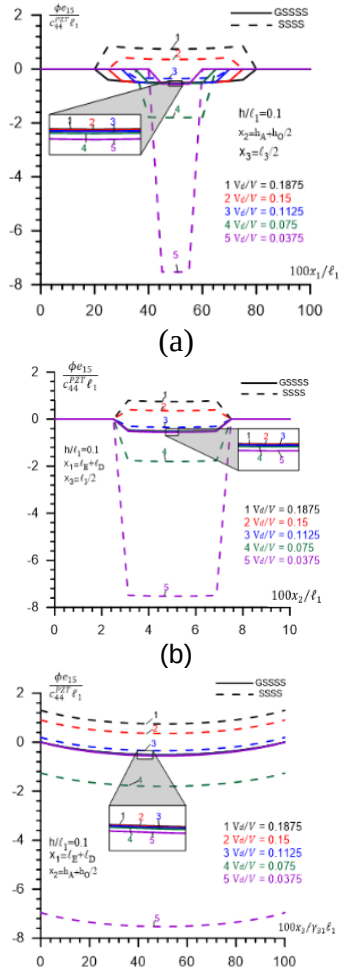

(a)

(b)

(c)

Fig. 10. Influence of V_D/V on the electric potential ϕ for PZT-5H inclusion/Al matrix material for both problems along the a) $0x_1$ axis b) $0x_2$ axis c) $0x_3$ axis.

In Figure 11, the effect of the polarization direction change on electric potential along the axis a) $\mathbf{Ox_1}$, for $\mathbf{x_2 = h_A + h_O/2}$, $\mathbf{x_3 = \ell_3/2}$, b) $\mathbf{Ox_2}$, for $\mathbf{x_1 = \ell_E + \ell_D}$, $\mathbf{x_3 = \ell_3/2}$ c) $\mathbf{Ox_3}$, for $\mathbf{x_1 = \ell_E + \ell_D}$, $\mathbf{x_2 = h_A + h_O/2}$ for PZT-5H inclusion/Al matrix material for both

problems are investigated. According to the graphs given in Figure 11-c, the greatest change in electric potential occurs in the direction of polarization parallel to the loading, i.e., for $\boldsymbol{Ox_2}$ polled direction. However, the following relationship can be written for the electric potential's values obtained in different polarization directions;

For Problem 2:

$$(\phi)_{Ox_1} > (\phi)_{Ox_2} > (\phi)_{Ox_3}$$

For Problem 1:

$$(\phi)_{Ox_2} > (\phi)_{Ox_1} \approx (\phi)_{Ox_3}$$

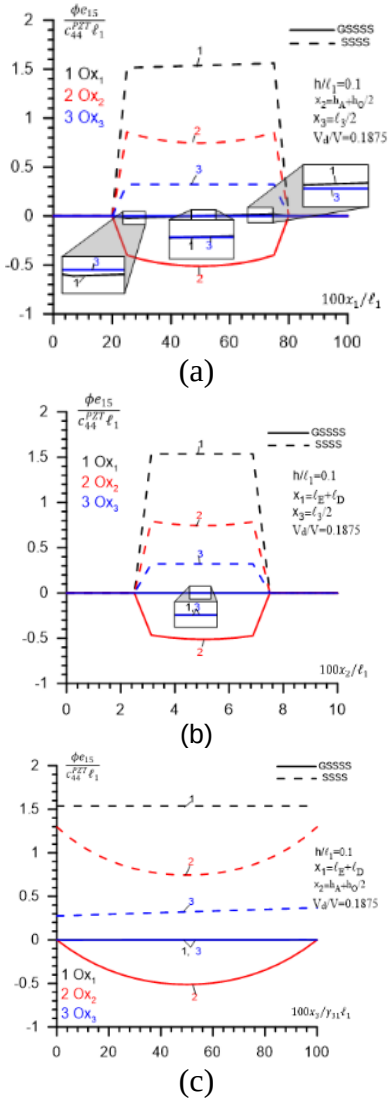

Fig. 11. Influence of polarization direction on the electric potential ϕ for PZT-5H inclusion/Al matrix material for both problems along the a) $0x_1$ axis b) $0x_2$ axis c) $0x_3$ axis.

The effect of the polarization direction change on a) the stress concentration $\boldsymbol{\sigma_{11}}$ along the $\mathbf{Ox_1}$ axis in the cross section of $\mathbf{x_2 = h_A + h_0/2}$, $\mathbf{x_3 = \ell_3/2}$ and on b) the displacement $\mathbf{u_2}$ along $\mathbf{Ox_2}$ axis in the cross section of $\mathbf{x_1 = \ell_E + \ell_D}$, $\mathbf{x_3 = \ell_3/2}$, for PZT-5H inclusion/Al matrix material for both problems are investigated in Figure 12. Both the absolute values of stress and displacement concentrations take their absolute minimum (maximum) values for $\mathbf{Ox_2}$ ($\mathbf{Ox_1}$) polled axis. And the difference of both problems are approximately same for the distributions.

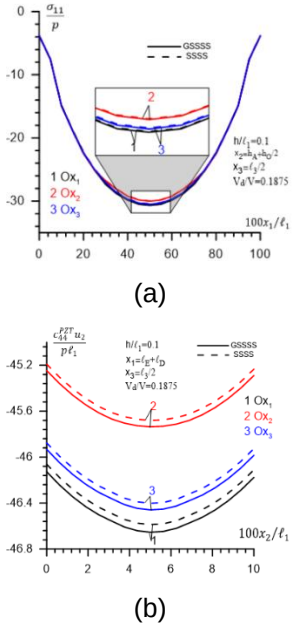

Fig. 12. Influence of polarization direction on the a) Stress concentration of σ_{11} along $0x_1$ axis b) Displacement of u_2 along $0x_2$ axis for PZT-5H inclusion/Al matrix material for both problems.

Figure 13 shows the influence of the location of the piezoelectric inclusion (i.e., increasing the parameter $\mathbf{h_A/\ell_1}$) on the electric potential along the axis a) $\mathbf{Ox_1}$ for $\mathbf{x_2 = h_A + h_0/2}$, $\mathbf{x_3 = \ell_3/2}$, b) $\mathbf{Ox_2}$ for $\mathbf{x_1 = \ell_E + \ell_D}$, $\mathbf{x_3 = \ell_3/2}$ c) $\mathbf{Ox_3}$ for $\mathbf{x_1 = \ell_E + \ell_D}$, $\mathbf{x_2 = h_A + h_0/2}$ for inclusion made PZT-5H material with $\mathbf{Ox_2}$ polled axis and Al matrix material for both problems are investigated. It can be seen from the plots that as the inclusion approach to the upper surface i.e. increasing $\mathbf{h_A/\ell_1}$ the absolute values of the electric potential decrease along the entire axis.

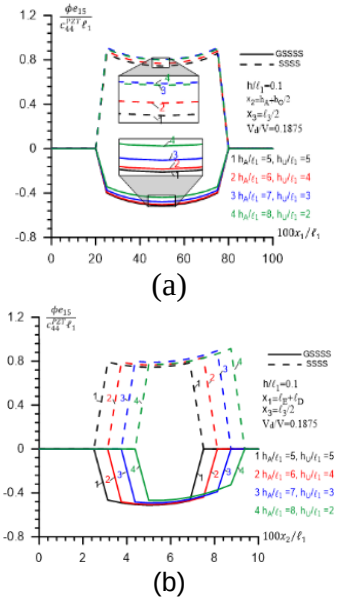

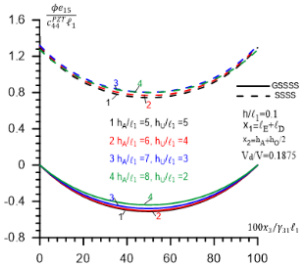

(c)

Fig. 13. Influence of h_A/ℓ_1 on the electric potential ϕ for PZT-5H inclusion/Al matrix material for both problems along the a) Ox_1 axis b) Ox_2 axis c) Ox_3axis.

The influence of the parameter $\mathbf{h_A/\ell_1}$ on a) the stress concentration of $\boldsymbol{\sigma_{11}}$ along the $\mathbf{Ox_1}$ axis in the cross section of $\mathbf{x_2 = h_A + h_O/2}$, $\mathbf{x_3 = \ell_3/2}$ and on b) the displacement of $\mathbf{u_2}$ along $\mathbf{Ox_2}$ axis in the cross section of $\mathbf{x_1 = \ell_E + \ell_D}$, $\mathbf{x_3 = \ell_3/2}$, for PZT-5H inclusion/Al matrix material for both problems are investigated in Figure 14.

Both the absolute values of displacement and stress concentrations decrease with increasing the parameter $\boldsymbol{h_A/\ell_1}$.

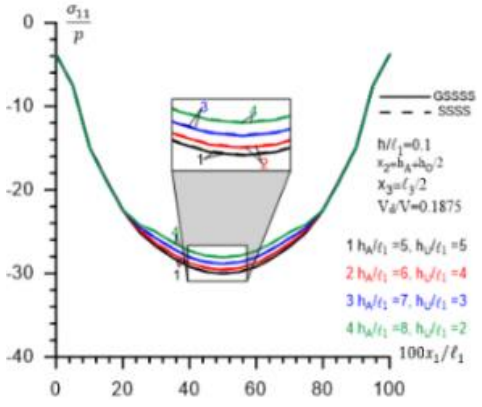

(a)

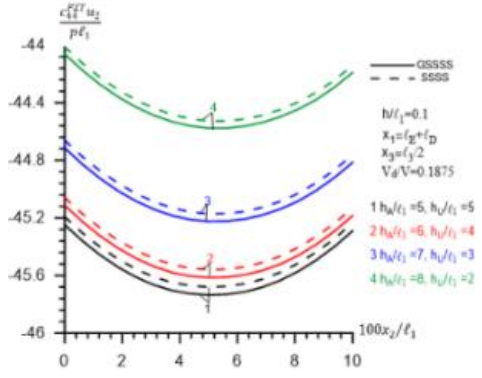

(b)

Fig. 14. Influence of h_A/ℓ_1 on the a) Stress concentration of σ_{11} along Ox_1 axis b) Displacement of u_2 along Ox_2 axis for PZT-5H inclusion/Al matrix material for both problems.

IV. CONCLUSIONS

The electrostatic analysis of the rectangular prismatic shape of the grounded and ungrounded thick composite plate with piezoelectric inclusion under bending force is solved using the Finite Element Method, with 3D exact equations of the theory of electroelasticity. The effects of constituent materials (inclusion and matrix), location and size of the piezoelectric inclusion on the electric potential, stress and displacement concentrations in the structure are analyzed and the following conclusions can be drawn:

- Whether the plate is grounded (Problem 1) or ungrounded (Problem 2) is very effective on the generation of the electric potential,
- The choice of piezoelectric material to obtain more electric potential may differ for grounded (Problem 1) and ungrounded (Problem 2) plate,
- Different material selection influences the values of electric potential in Problem 2 more than in Problem 1,
- By selecting PZT-5A (PMN-PT) material for inclusion, maximum (minimum) stresses and displacements are obtained,
- The stress concentration do not differ in both problems,
- The displacement concentration is slightly larger in Problem 1 than Problem 2,
- The largest absolute value of the electric potential according to the matrix material selection is obtained in Problem 2 for St material, in Problem 1 for Mg material,
- Electric potential decrease with the size of the PZT inclusion in the plate,
- The greatest change in electric potential occurs in the direction of polarization parallel to the loading, i.e., for $\mathbf{Ox_2}$ polled direction,
- The absolute values of the electric potential, stress and displacement concentrations decrease as upward shift of the position of the piezoelectric inclusion.

ACKNOWLEDGMENT

This work is supported by the Scientific and Technological Research Council of Turkey (TUBITAK) within the scope of "2209-A University Students Research Projects Support Program" under the Grant Number: 1919B012301237).

REFERENCES

[1] J. Tichy, J. Erhart, E. Kittinger, J. Privratska, *Fundamentals of Piezoelectric Sensorics: Mechanical, Dielectric and Thermodynamical Properties of Piezoelectric Materials*, Springer, 2010.

[2] B. Wang, "Three-dimensional analysis of an ellipsoidal inclusion in a piezoelectric material," *International Journal of Solids and Structure*, vol. 29, pp. 293-308, 1992.

[3] Y.E. Pak, "Circular inclusion problem in antiplane piezoelectricity," *International Journal of Solids and Structure*, vol. 29(19), pp. 2403–2419, 1992.

[4] H. Fan, S. Qin, "A piezoelectric sensor embedded in a non-piezoelectric matrix," *International Journal of Engineering Science,* vol. 33, pp.379-88, 1995.

[5] P. Lu, F.W. Williams, "Green functions of piezoelectric material with an elliptic hole or inclusion," *International Journal of Solids and Structure*, vol.35(7–8), pp. 651–664, 1998.

[6] Z.M. Xiao, J. Bai, "On piezoelectric inhomogeneity related problem-part I: a close-form solution for the stress field outside a circular piezoelectric inhomogeneity," *International Journal of Engineering Science*, vol. 37, pp.945-59, 1999.

[7] Q.H. Qin, "Green function and its application for a piezoelectric plate with various openings," *Archive of Applied Mechanics*, vol.69, pp.133–144, 1999.

[8] L. Dai, W. Guo, X. Wang, "Stress concentration at an elliptic hole in transversely isotropic piezoelectric solids," *International Journal of Solids and Structure*, vol.43, pp.1818–1831, 2006.

[9] Y. Gao, M. Wang, B. Zhao, "The remarkable nature of radially symmetric deformation of anisotropic piezoelectric inclusion," *Acta Mechanica Solida Sinica*, vol. 21, pp.278-82, 2008.

[10] D. Mishra, C.Y. Park, S.H. Yoo, Y.E. Pak, "Closed-form solution for elliptical inclusion problem in antiplane piezoelectricity with far-field loading at an arbitrary angle," *European Journal of Mechanics A/Solids*, vol.40, pp.186-97, 2013.

[11] Y E. Pak, "Elliptical inclusion problem in antiplane piezoelectricity: implications for fracture mechanics," *International Journal of Engineering Science,* vol. 48, pp. 209–222, 2010.

[12] D. Mishra, S.H. Yoo, C.Y. Park, Y.E. Pak, "Elliptical Inclusion Problem In Antiplane Piezoelectricity: Stress Concentrations and Enegy Release Rates," *International Journal of Fracture*, vol. 179, pp. 213-20, 2013.

[13] Y.T. Lee, J.T. Chen, S.R. Kuo, "Null-field integral approach for the piezoelectricty problems with multiple elliptical inhomogeneties," *Engineering Analysis with Boundary Elements,* vol. 39, pp. 111-20, 2014.

[14] M. Dai, C.F. Gao, "Perturbation solution of two arbitrarily-shaped holes in a piezoelectric solid," *International Journal of Mechanical Sciences*, vol. 88, pp. 37–45, 2014.

[15] B.H. Yang, C.F. Gao, "Anti-plane problems of a piezoelectric inclusion with an elliptical hole or a crack in an infinite piezoelectric matrix," 2015 Symposium on Piezoelectricity; Acoustic Waves, and Device Applications, Jinan, China, 2015.

[16] H. Sosa, "Plane problems in piezoelectric media with defects," *International Journal of Solids and Structure*, vol. 28, pp. 491–505, 1991.

[17] B.H. Yang, C.F. Gao, "Plane problems of multiple piezoelectric inclusions in a non-piezoelectric matrix". *International Journal of Engineering Science*, vol. 48, pp. 518-28, 2010.

[18] R. Jerome, N. Ganesan, "New generalized plane strain FE formulation for the buckling analysis of piezocomposite beam," *Finite Elements in Analysis and Design*, vol. 46, pp.896–904, 2010.

[19] X. Wang, Y. Zhou, W. Zhou, "A novel hybrid finite element with a hole for analysis of plane piezoelectric medium with defects," *International Journal of Solids and Structure*, vol. 41, pp. 7111– 7128, 2004.

[20] Z.D. Zhou, S.X. Zhao, Z.B. Kuang, "Stress and electric displacement analyses in piezoelectric media with an elliptic hole and a small crack," *International Journal of Solids and Structure*, vol. 42, pp. 2803–2822, 2005.

[21] S.C. Obilikpa, U.P. Onochie, C.S. Nweze, B.O. Kalu and K.B.I. Anazodo, "Design and Numerical Simulation of a Novel High-Speed Multi-Degrees of Freedom Piezoelectric positioner," *Journal of Applied Science and Engineering*, vol. 24 (3), pp. 407-414, 2021.

[22] Q. Lu, X. Chen, W. Huang, "A novel rhombic piezoelectric actuator applied in precision positioning stage," *Journal of Applied Science and Engineering*, vol. 23(3), pp.405–411, 2020.

[23] M.A. Trindade, A. Benjeddou, "Parametric analysis of effective material properties of thickness-shear piezoelectric macro-fibre composites," *Journal of The Brazilian Society of Mechanical Sciences and Engineering,* vol. 34, pp.352-361, 2012.

[24] V. Tita, R. Medeiros, F.D. Marques, M.E. Moreno, "Effective properties evaluation for smart composite materials with imperfect fiber–matrix adhesion" *Journal of Composite Materials*, vol. 49(29), pp. 3683-3701, 2015.

[25] U. Babuscu Yesil, N. Yahnioglu, Y. Ucan, "Electrostatic analysis of rectangular thick plate containing piezoelectic prismatic inclusion wıth FEM". *Nigde Omer Halisdemir University Journal of Engineering Sciences*, vol.8, pp.69-81, 2019.

[26] Z. Gong, Y. Zhang, E. Pan, C. Zhang, "Field concentration and distribution in three-dimensional magneto-electroelastic plates with open holes," *European Journal of Mechanics A/Solids*, 99, 104914, 2023.

[27] A. Kevin, M. Akbar, L. Gunawan, D.K. Aulia, R. Agung, S.S. Rawikara, et all., "Evaluation of Piezoelectric-based Composite for Actuator Application via FEM with Thermal Analogy," *European Journal of Computational Mechanics*, vol.32(5), pp. 495–518, 2023.

[28] U. Babuscu Yesil, F. Aylikci, "3D FEM analysis of stress concentrations in a rectangular thick plate with PZT inclusions under bending," *Sigma Journal of Engineering and Natural Sciences*, vol. 41(6), pp. 1−12, 2023.

[29] O.C. Zienkiewicz, R.L. Taylor, *The Finite Element Methods: Basic Formulation and Linear Problems*, McGraw-Hill Book Company, Oxford, 1989.

[30] J. Yang, *An Introduction to The Theory of Piezoelectricity*, Springer, 2005.

[31] H.F. Tiersten, *Linear piezoelectric plate vibrations*, New York, NY: Plenum, 1969.

[32] N. Yahnioğlu, *Analysis of boundary value problems suitable for the statics of structural elements prepared from composite materials with a curvilinear structure using FEM*. PhD Thesis, Yildiz Technical University, Istanbul, 1996.